Journal of Applied Physics

Dopant profiling in *p-i-n* GaN structures using secondary electrons

Cite as: J. Appl. Phys. **126**, 015704 (2019); https://doi.org/10.1063/1.5096273
Submitted: 15 March 2019 . Accepted: 17 June 2019 . Published Online: 02 July 2019

Shanthan R. Alugubelli, Houqiang Fu, Kai Fu, Hanxiao Liu, Yuji Zhao, and Fernando A. Ponce

AIP Publishing

Journal of Applied Physics ARTICLE scitation.org/journal/jap

Dopant profiling in *p-i-n* GaN structures using secondary electrons

Cite as: J. Appl. Phys. **126**, 015704 (2019); doi: 10.1063/1.5096273
Submitted: 15 March 2019 · Accepted: 17 June 2019 ·
Published Online: 2 July 2019

Shanthan R. Alugubelli,[1] Houqiang Fu,[2] Kai Fu,[2] Hanxiao Liu,[1] Yuji Zhao,[2] and Fernando A. Ponce[1,a)]

AFFILIATIONS

[1]Department of Physics, Arizona State University, Tempe, Arizona 85287, USA
[2]School of Electrical, Computer and Energy Engineering, Arizona State University, Tempe, Arizona 85287, USA

[a)]**Email address:** ponce@asu.edu

ABSTRACT

We show that secondary electrons in a scanning electron microscope can provide important information about spatial dopant distribution in *p-i-n* GaN structures, with the highest contrast observed for a primary electron beam accelerating voltage in the range of 1 to 2 kV. The current through the specimen is used to determine the total backscattered and secondary electron yield. We establish a correlation between the secondary electron emission intensity and the doping characteristics of the material. The secondary electron emission intensity was found to be highest for *p*-type GaN, intermediate for *n*-type GaN, and lowest for undoped GaN. Specimen currents are found to have a strong correlation with the Mg concentration in *p*-GaN films. The contrast associated with dopants is shown to depend on experimental parameters such as primary electron beam voltage, total electron beam exposure, and specimen surface history. This technique can serve as a powerful tool for the development and characterization of thin films for GaN power electronics.

I. INTRODUCTION

Semiconductor devices for power applications require materials with high electron mobility and high breakdown electric field,[1] which result in faster switching speeds, lower switching losses, and compact device size.[1,2] Gallium nitride is a wide bandgap material of great interest due to its higher breakdown electric fields (3.3–3.75 MV/cm) when compared to silicon (0.3 MV/cm). GaN thin films grown on sapphire have a suboptimal power device performance due to high dislocation densities (10^8–10^{10} cm^{-2}).[1] The availability of GaN substrates has led to the development of vertical GaN-on-GaN power devices with dislocation densities of about 10^6 cm^{-2}, resulting in improved performance.[3,4]

The background impurity concentration in GaN films grown by metalorganic chemical vapor deposition (MOCVD) is typically in the range of 10^{15}–10^{17} cm^{-3}, depending on the condition of the reactor, and therefore, undoped GaN (*i*-GaN) usually presents *n*-type conductivity. Silicon and magnesium are commonly used as *n*-type and *p*-type dopants in GaN. Silicon acts as a donor with an ionization energy of about 25 meV, and device quality *n*-type GaN is typically doped with Si at about 10^{18} cm^{-3}, resulting in donor concentrations of about the same order of magnitude. The situation is different for *p*-type doping: Mg acts as an acceptor in GaN with an ionization energy of about 200 meV. Thermal annealing at about 750 °C results in 1% to 2% ionized acceptors at room temperature. Typically, Mg-doping levels at about 10^{19} cm^{-3} result in acceptor concentrations in the low 10^{17} cm^{-3}.[5] Mg-dopant concentrations below 10^{19} cm^{-3} are of little practical use in devices because the material is too resistive. Also, Mg concentration levels above 10^{20} cm^{-3} result in lower conductivity and in Mg-precipitation.[6] Anisotropy in the wurtzite crystal structure leads to a dependence of the Mg-doping efficiency on the crystal orientation, such as in the case of growth on etched mesa structures.[5] Identification with submicrometer spatial resolution of the Mg distribution in the mesa structures is important in order to understand the device performance characteristics.

High power devices, such as vertical-junction field-effect transistors (VJFETs), superjunctions (SJs), and junction-barrier Schottky (JBS) diodes, consist of laterally patterned *p-i* or *p-n* junctions.[2] Lateral patterns are typically achieved via etch-and-regrowth or by ion implantation and annealing.[7,8] For example, a VJFET has a *p*-GaN region as the gate, an intrinsic region as the drift layer, and *n*-GaN regions acting as source and drain. A significant variation in the electronic properties of Mg-doped GaN has been observed by cathodoluminescence spectroscopic imaging,[5] which has been attributed to changes in the crystallographic orientation

during growth. Knowledge of variations from the intended layer design is helpful in understanding device performance and failure mechanisms. Secondary ion mass spectroscopy (SIMS), routinely used for quantification of dopants in semiconductors, cannot resolve lateral variations, posing a significant challenge in the development of advanced GaN power devices.

We report here on a quantitative approach using secondary electrons (SE) for determining both the lateral and vertical dopant distribution profiles in *p-i-n* GaN structures at a submicrometer scale. The SE emission in a material involves three steps, starting with the generation of SEs inside the bulk by the incident primary electrons, their transport toward the surface, and their emission by escape into vacuum.[9,10] These steps depend on the diffusion length of electrons in the bulk, the mean escape depth of electrons near the surface, the band bending due to surface states, and the chemical nature of the surface.[9,11–13] The electron transport properties and the nature of the surface states depend on the doping characteristics of the semiconductor and the chemical nature of the surface. This results in a dependence of the secondary electron emission on doping levels and on sample surface preparation.

Owing to differences in secondary electron detectors and their placement geometries (angle, distances, scintillator design) relative to the sample stage, the data obtained are not quantitatively accurate, but contrast can be observed under selected conditions. A standard Everhart-Thornley (E-T) type SE detector is commonly used for profiling/imaging, in cross section at a submicrometer scale, the lateral and vertical dopant distributions in *p-i-n* GaN structures. To obtain reliable quantitative measurements, we use the specimen itself as a detector,[14,15] to measure the current through the specimen and to plot the variation of SE yields with accelerating voltage. The specimen current maintains charge neutrality in the semiconductor, as depicted in Fig. 1. The SE yield is defined as the number of secondary electrons emitted corresponding to each incident primary electrons. The differences in the SE yields, obtained from specimen current measurements, can be used to explain the observed dopant contrast in *p-i-n* GaN structures. The SE emission for differently doped GaN has a strong dependence on the primary electron beam voltage, with the highest contrast observed at low electron beam voltages.[12,13,16–18] We observe a strong correlation between electron yields and the Mg concentration in *p*-GaN. We show that this method can potentially augment the existing quantification methods.[19,20]

We analyze the effect of experimental parameters such as electron beam voltage, exposure dose, and specimen surface history on the SE emission contrast associated with dopants. We find that low voltages in the range of 1–2 kV optimize the contrast between differently doped regions. *p*-type regions have the highest SE emission, followed by *n*-type regions, and the lowest for undoped regions. Surface conditions have to be optimal to retrieve any meaningful information from SE micrographs. Lower exposure times and smaller dwell times tend to show higher contrast.

II. EXPERIMENTAL DETAILS

A. Thin film growth and specimen preparation for SEM

The samples under investigation were grown by metalorganic chemical vapor deposition (MOCVD) on an *n*-type GaN substrate with a carrier concentration of $\sim 10^{18}\,\mathrm{cm}^{-3}$. The precursors were trimethylgallium (TMGa) and ammonia (NH_3), with H_2 as the carrier gas. Bis(cyclopentadienyl)magnesium (Cp_2Mg) and silane (SiH_4) were the sources for Mg and Si.[21] Cross-section samples for SEM were prepared by mechanical polishing with diamond lapping films down to a grit size of 0.1 μm using a tripod polishing tool. Standard cleaning procedures with organic solvents were used. The samples were dipped in a 1:10 HF solution in de-ionized water to remove residual surface oxidation and then mounted on a SEM stub using a carbon tape. Silver paste was used to ground the sample to avoid charging effects.

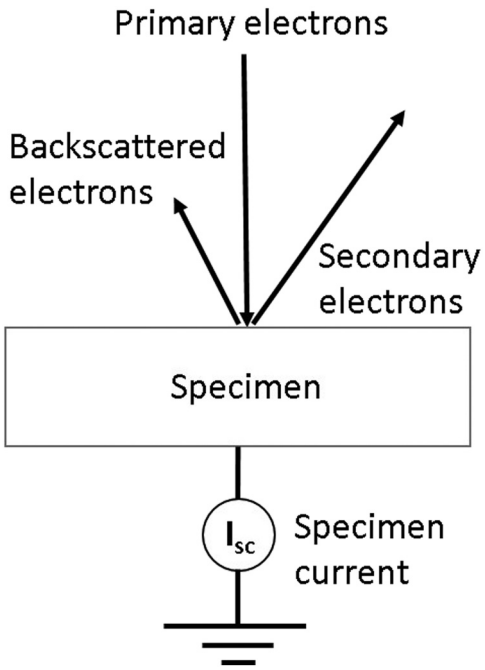

FIG. 1. Schematic diagram of electrons flowing in and out of a specimen in an SEM.

B. Secondary electron detection and imaging

Two types of detectors were used to study the interaction of primary electrons with the specimen. One is the SE detector for imaging the spatial variation of dopant contrast, and the other is the specimen itself as a detector to measure the specimen current and quantify the total backscattered and secondary electron emissions.

The SE detector is of the Everhart-Thornley (E-T) type, which uses a scintillator with a thin metal coating biased at a positive potential of about 10 kV to detect low-energy secondary electrons. The signal obtained is a convolution of SEs from the beam-specimen interaction and backscattered electrons (BSEs) originating from the specimen and from the chamber wall, all traveling within the solid angle of the detector.[11] The E-T detector design characteristics, such as solid-angle coverage and signal amplification, are not suitable for the measurement of the absolute number of emitted

electrons. Nevertheless, the E-T detector provides information about dopant distribution in GaN *p-i-n* structures. Contribution of BSEs to the SE signal can be reduced by utilizing a lens detector or an upper SE detector, which utilizes the magnetic field projected by the objective lens to draw the SE electrons.

The secondary electron images in this study were collected in an FEI XL 30 sFEG microscope, operated at working distances of ~3–5 mm, using an E-T SE detector. The working distance was kept as short as possible to optimize secondary electron collection efficiency.

C. The specimen as a detector

In an SEM, the specimen itself can be used as a detector by measuring the current passing through it.[14] The specimen current represents the difference between the primary beam current and the SE and BSE currents, as depicted in Fig. 1. Charge neutrality under steady state conditions requires

$$I_{SE} + I_{BSE} = I_b - I_{sc}, \quad (1)$$

where I_{SE} is the secondary electron current, I_{BSE} is the backscattered electron current, I_b is the primary electron beam current, and I_{sc} is the current passing through the specimen. Equation (1) can also be expressed in terms of secondary electron yield ($\delta = I_{SE}/I_b$) and backscattered electron yield ($\eta = I_{BSE}/I_b$) as follows:

$$\delta + \eta = 1 - I_{sc} / I_b. \quad (2)$$

The BSE yields are low ($\eta \leq 0.3$) for elements with an atomic number of about 38,[11] and relatively constant as a function of primary electron beam accelerating voltage.[22] Therefore, back scattered electrons appear as a low and constant background, and the electron emission yields measured in this study reflect the variations of the SE yields with accelerating voltage.

Specimen current measurements were done in an FEI Nova Nano-lab 200 microscope, with the primary electron beam accelerating voltage varying from 0.25 to 12 kV, and the beam currents in the 30–50 pA range. This instrument does not have the capability to record the specimen current in a matrix format. The SE images in this paper were obtained using the XL-30 microscope described earlier.

III. RESULTS AND DISCUSSION

A. Dopant contrast using SE detector at various primary electron beam energies

An SE image acquired at 2 kV from an as-polished surface of a *p-i-n* GaN thin film structure is shown in Fig. 2. The emission intensity is highest for the *p*-layer, followed by the *n*-layer, and it is lowest for the *i*-layer. The insets in Fig. 3(b) show SE images of *p-i-n* structures at 0.25, 2.0, and 5 kV. The contrast between the undoped and the *n*-type layers vanishes when the voltage is increased from 2 kV to 5 kV, as shown in the inset of Fig. 3(b).

The choice of the primary electron beam accelerating voltage is crucial for optimizing dopant contrast in *p-i-n* GaN thin film structures. The relative SE emission intensities from different layers

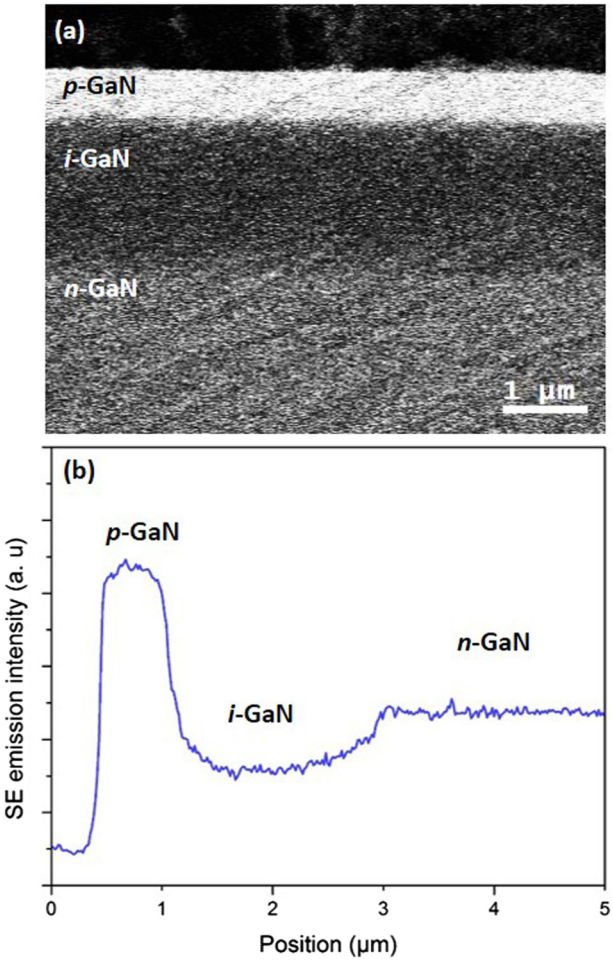

FIG. 2. SE image and the SE emission intensity profile of the *p-i-n* GaN structure, acquired at a primary electron beam energy of 2 kV and a beam current of 53 pA.

depend on the primary electron beam accelerating voltage. In order to avoid contrast inversion, and to distinguish all layers, electron beam voltages in the range of 1.5–2 kV are preferred. Accelerating voltages below 1 kV can cause a contrast inversion between the *p*-type and the *n*-type layers if the electron dose is higher.

B. SE yield dependence on primary electron beam energy for *p*-GaN, *i*-GaN, and *n*-GaN

Electron yields for *p*-GaN, *n*-GaN, and *i*-GaN are plotted in Fig. 3(a). The electron yield is highest for *p*-GaN, followed by *n*-GaN, and it is lowest for *i*-GaN. The maximum electron yield occurs at ~1.25 kV for *p*-GaN and at ~0.5 kV for both *i*-GaN and *n*-GaN. The difference in electron yields for *p*-GaN and *n*-GaN is shown in Fig. 3(b). Yield difference for *p*-GaN and *n*-GaN is highest for the voltage range of 1–2 kV. It is important to note that

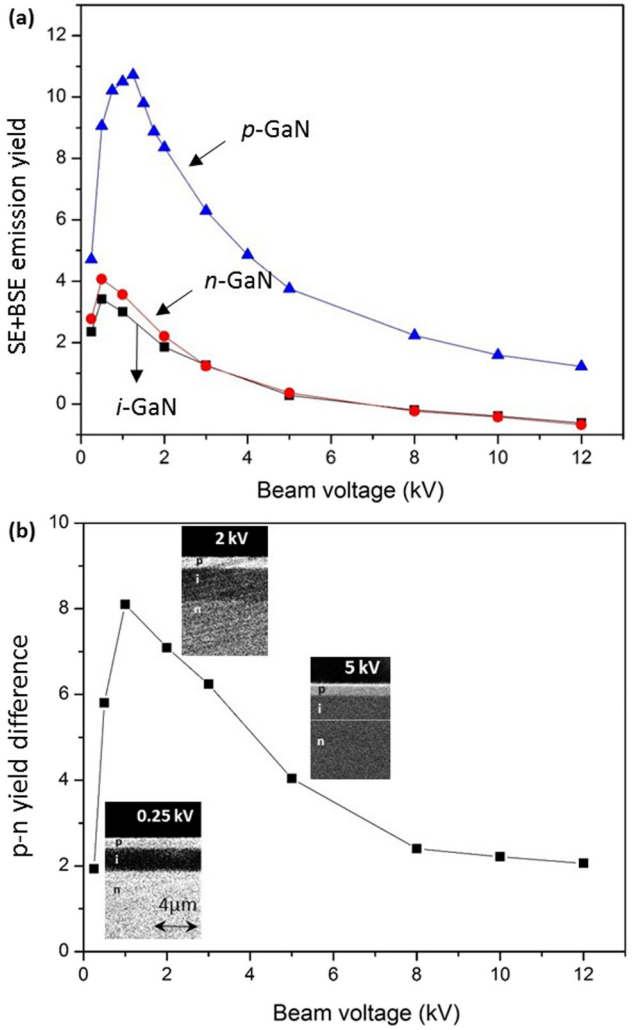

FIG. 3. (a) Variation in electron emission yields for *p*-GaN, *n*-GaN, and *i*-GaN plotted for primary electron beam energies ranging from 0.25 kV to 12 kV. (b) SE yield difference between *p*-GaN and *n*-GaN as a function of electron beam energies. The inset shows variation in SE image intensities in the *p-i-n* structure at 0.25 kV, 2 kV, and 5 kV.

the yield difference does not have any contribution from BSEs, since BSEs should be independent of doping. Also, the electron yields for the *i*-GaN and the *n*-GaN are equal for the voltages above 3 kV. This can be observed in the SE images in the inset of Fig. 3(b), where the contrast between the *i*-GaN and the *n*-GaN vanishes at 5 kV. The electron yield measurements for our case are similar to the measurements reported by Yater *et al.*[23]

The dependence of the SE yield with primary electron beam voltage is similar for most materials.[24] The yield initially increases up to a maximum value, and then decreases with voltage.[11] This is related to the penetration depth of the primary electrons and to the escape depth of the secondary electrons. The penetration depth increases with beam voltage, and the total number of local secondary electrons increases with excitation volume. Below the voltage at maximum electron yield (V_m), the penetration depth is lower than the escape depth of secondary electrons, resulting in the secondary electrons escaping into vacuum. The penetration depth and escape depth are equal at V_m. Above V_m, the penetration depth is higher than the escape depth of the secondary electrons, resulting in many SEs losing energy before reaching the surface. Therefore, for voltages greater than V_m, the electron yields are lower despite the higher number of secondary electrons generated inside the material.

There are two possible explanations for the dopant contrast mechanism. First, Perovic *et al.*[12] attributed the dopant contrast observed in silicon to the band bending near the bulk-vacuum interface due to the presence of surface states. Later, Sealy *et al.*[13] attributed the observed contrast in silicon to differences in ionization energies of differently doped regions due to the built-in potential near the surface. Volotsenko *et al.*[20] used semiempirical one-dimensional constant loss theory proposed by Dionne[24] to simulate the dopant contrast observed in silicon. They found that the escape depth parameter is the major factor influencing the dopant contrast. The escape depth depends on the electric fields induced by the surface band bending, which varies with the dopant type and concentration. The concept of ionization energy does not seem to apply to our case since *i*-GaN has the lowest SE emission (*i*-GaN would be expected to be between the *p*- and *n*-GaN), as explained next. The lower SE yield for *i*-GaN can be attributed to its inability to replenish some of the SE electrons because of the lower conductivity.[25] In the case of *p*-GaN and *n*-GaN, surface states result in downward and upward band bending near the surface, respectively.[26,27] Using photoelectron and X-ray photoemission spectroscopies at low temperatures, $E_f - E_v$ at the surface has been reported to be about 2.7 eV for *n*-type GaN and about 1.3 eV for *p*-type.[26,28,29] These values correspond to upward band bending of 0.7 eV for *n*-type and downward band bending of 1.1 eV for *p*-type, as shown schematically in Fig. 4. Downward band bending near the surface of *p*-GaN contributes to electron transport toward the surface, thus enhancing SE emission. On the other hand, upward band bending near the surface of *n*-GaN tends to deplete electrons from the surface, thus diminishing SE emission.[12,20]

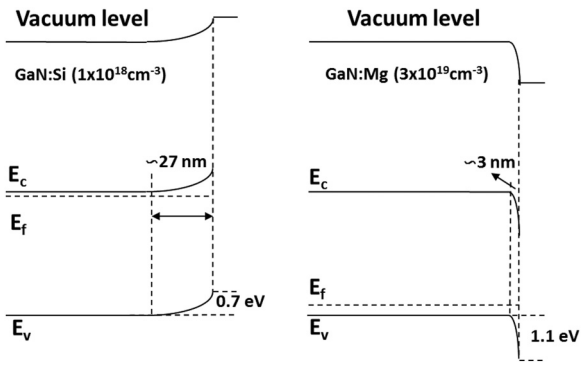

FIG. 4. Schematic diagram of electronic band bending near the surface for *p*-GaN and *n*-GaN.

C. SE yield dependence on Mg concentration in *p*-GaN

Electron yields have a strong positive correlation with Mg concentration as shown in Fig. 5(a). Figure 5(b) shows the SE emission intensity recorded with an SE detector for *p*-GaN films with different Mg concentrations. The inset shows the relative contrast for the three *p*-GaN films.

The signal recorded using an SE detector is not absolute since it depends on the detector sensitivity, its collection solid angle, and several operational microscope parameters. Therefore, the quantification from the intensities recorded can only be relative.[17,18,30] On the other hand, the difference between beam and specimen currents provides an absolute value for the total number of emitted (BSE and SE) electrons, as represented in Fig. 1. This method can potentially be used for quantitative dopant profiling of *p*-GaN by first calibrating the electron yields with different Mg concentrations.

D. Effect of the nature of the surface on secondary electron emission

The nature of surface is critical in order to observe the maximum dopant contrast. Figure 6 shows the effects of air and UV exposure on the SE emission from *p-i-n* GaN thin film structures. A clear reduction in contrast is observed in both cases. HF treatment on a UV exposed surface restores the contrast between layers.

The SE emission contrast is highest in *p-i-n* GaN thin film structures for as-polished samples [Fig. 2(a)]. We believe that oxidation of the surface tends to diminish the contrast observed

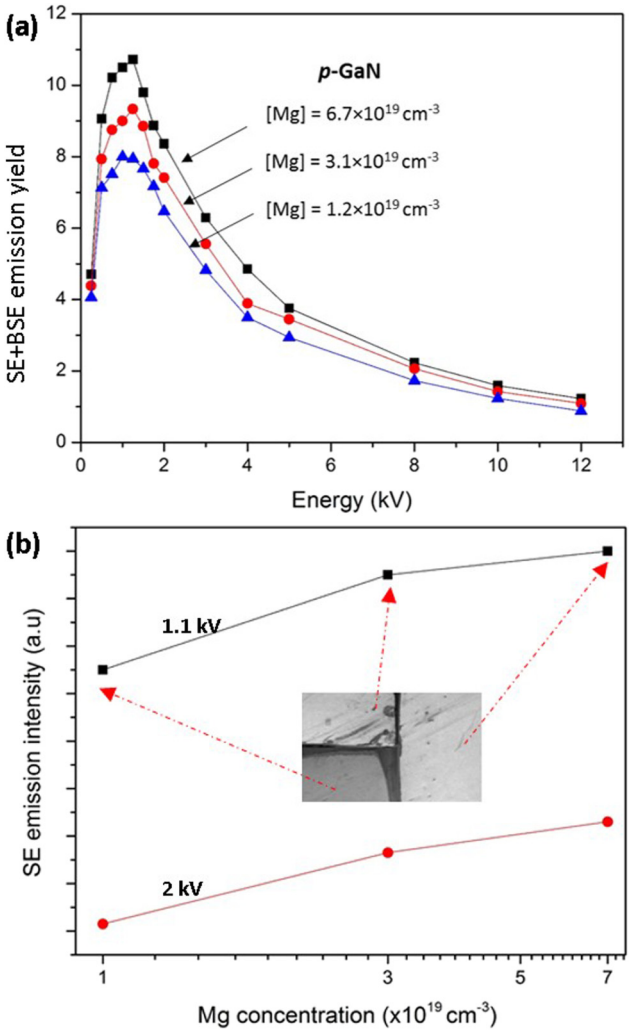

FIG. 5. Electron emission characteristics for Mg-doped GaN. (a)Variation in electron emission yields as a function of primary electron beam energy for various Mg concentrations. (b) SE emission intensity dependence on the Mg concentration for different primary electron beam energies.

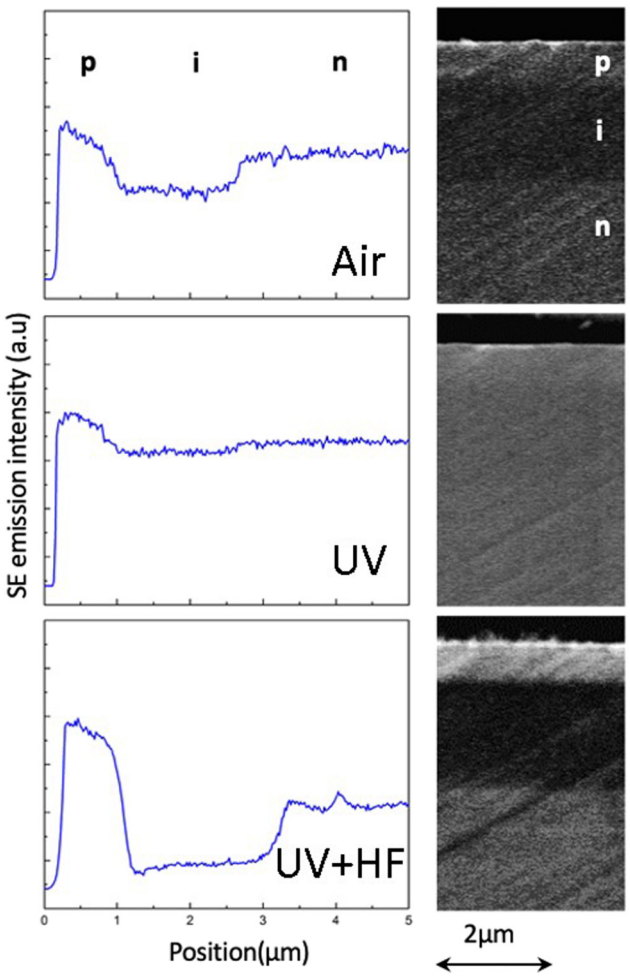

FIG. 6. SE emission intensity profiles and images of a *p-i-n* GaN structure with surfaces that were exposed to air for 2 days, exposed to UV for 2 h, and treated with HF after UV exposure.

between layers. Etching the oxide layer formed on the GaN surface using dilute HF restores the contrast between layers. Therefore, a clean surface is crucial for observing optimal dopant contrast.

E. Effect of beam dwell time and exposure time

For observing optimal dopant contrast, faster scan rates and lower exposure times are necessary. The contrast observed between *p*-GaN and *n*-GaN layers using an SE detector may be quantified as follows:

$$C_{pn} = \frac{I_p - I_n}{I_n},$$

where I_p and I_n are the recorded intensities from the *p*- and *n*-layers, respectively. Scan rates and exposure time have a significant effect on the dopant contrast.[31] The effect of electron beam dose on C_{pn} is plotted in Fig. 7(a). The dose is defined as the product of beam current per unit area and dwell time. The contrast decreases with increasing electron dose. The dependence of C_{pn} on beam exposure time is plotted in Fig. 7(b) for different electron beam voltages. We observe a gradual decrease in contrast with exposure time for 2 kV and 5 kV. The change in contrast could be due to the contamination build-up after prolonged beam exposures. For 10 kV, we observe an increase in contrast with time, which may be related to the penetration depth of about 700 nm. The diffusion length of electrons in *p*-GaN increases with time resulting in a higher number reaching the surface at prolonged exposures.[32] In conclusion, anomalies in the dopant contrast can be avoided by minimizing electron dose and exposure time.

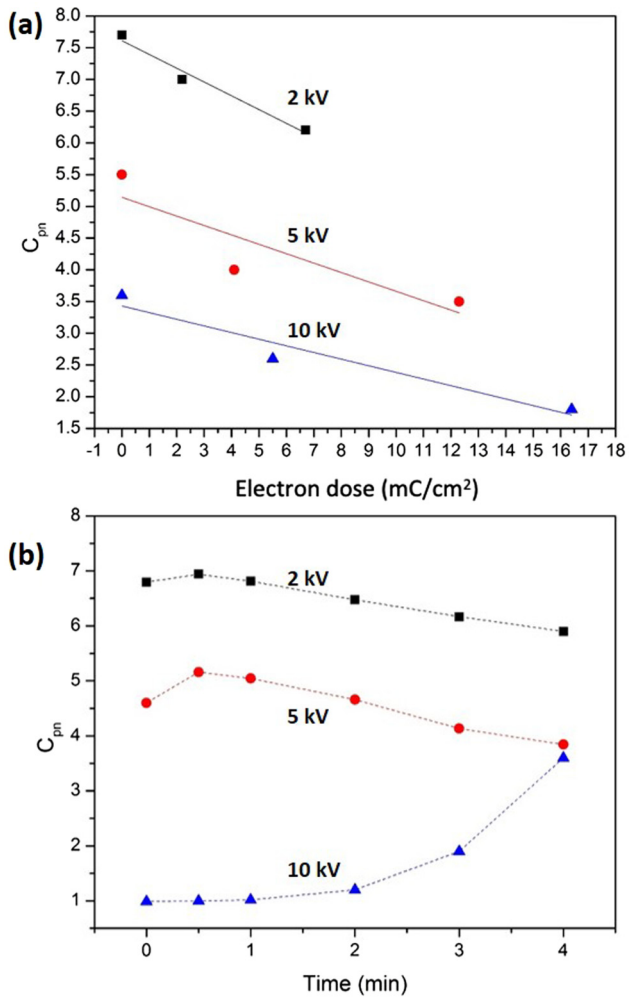

FIG. 7. SE emission contrast (C_{pn}) of *p-n* GaN structures, for primary electron beam energies of 2 kV, 5 kV, and 10 kV: (a) As a function of electron dose for a single scan. (b) As a function of total exposure time with an electron dose rate of 30 μC/cm^2 s. The raster area in these measurements is 15.5 × 11.7 μm^2.

F. Applications on high power devices

In power devices, lateral and vertical patterns of *p-i* and *p-n* junctions are used for power delivery. The patterns are produced by a variety of methods such as etch-and-regrowth of differently

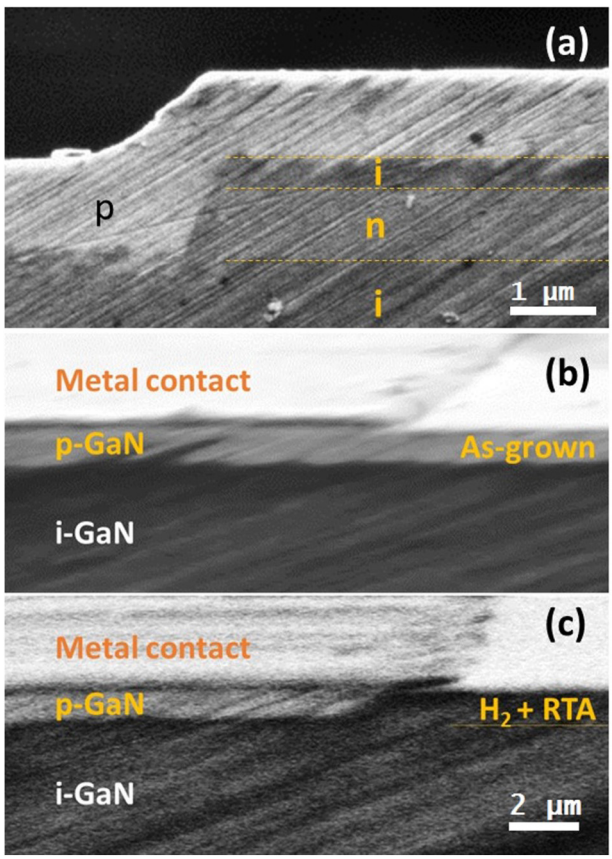

FIG. 8. SE images of (a) etched-and-regrown *p-i-n* GaN mesa structure, (b) as-grown *p*-GaN, and (c) H_2 implanted plus annealed *p*-GaN.

doped regions or by ion implantation. Devices require good edge definition of the differently doped regions. Faulty material results in high leakage currents and low reverse breakdown voltages. Direct visualization of the actual geometry of differently doped regions is important in order to understand the nature of the device structure and its performance.

We have utilized SE imaging to characterize selective area doping. For instance, the horizontal and vertical dopant distribution can be identified from the SE image of the *p-i-n* GaN etched mesa structure in Fig. 8(a). The dopant profiles are useful for understanding the growth mechanisms along different crystal orientations and the lateral electron transport properties. Another example is in the study of Mg passivation using a H_2 plasma treatment. Figure 8(b) shows an as-grown *p-i*-GaN junction partially covered with a metal contact. Figure 8(c) shows a similar region after the H_2 plasma treatment with thermal annealing, revealing a clear difference in the SE emission characteristics for the hydrogenated *p*-GaN region. The exposed *p*-GaN region is deactivated and exhibits *i*-type SE contrast. Edge termination using H_2 plasma treatment can potentially avoid etch damage and achieve lower leakage currents.[33]

IV. CONCLUSION

In summary, SE detectors have been used to obtain dopant profiles in *p-i-n* GaN structures. The SE emission intensity is highest from *p*-type GaN and lowest from undoped GaN. Variations in SE yields have been measured for *p*-GaN, *n*-GaN, and *i*-GaN using the specimen as a detector. These measurements show that low electron beam voltages maximize dopant contrast due to higher yield differences between *p*-GaN and *n*-GaN. The specimen current has a strong dependence on the Mg concentration in *p*-GaN films, which can potentially be utilized for quantitative dopant profiling in the SEM. Examples have been presented proving the technique's unique advantage in cross-section dopant profiling with a high spatial resolution. Regions with electrically inactive dopants can be identified as in the case of edge termination achieved by H_2 plasma and thermal annealing. SE imaging is a unique tool for visualizing dopant distribution in GaN with a high spatial resolution.

ACKNOWLEDGMENTS

We gratefully acknowledge valuable discussions with Professor Robert Nemanich. This work is supported by ARPA-E PNDIODES Program monitored by Dr. Isik Kizilyalli. We acknowledge the use of facilities within the Eyring Materials Center at Arizona State University. The device fabrication was performed at the Center for Solid State Electronics Research at Arizona State University. Access to the NanoFab was supported, in part, by the National Science Foundation (NSF) under Contract No. ECCS-1542160.

REFERENCES

[1]I. C. Kizilyalli, A. P. Edwards, O. Aktas, T. Prunty, and D. Bour, "Vertical power p-n diodes based on bulk GaN," IEEE Trans. Electron Devices **62**, 414 (2015).
[2]H. Amano, Y. Baines, E. Beam, M. Borga, T. Bouchet, P. R. Chalker, M. Charles, K. J. Chen, N. Chowdhury, R. Chu, C. De Santi, M. M. De Souza, S. Decoutere, L. Di Cioccio, B. Eckardt, T. Egawa, P. Fay, J. J. Freedsman, L. Guido, O. Häberlen, G. Haynes, T. Heckel, D. Hemakumara, P. Houston, J. Hu, M. Hua, Q. Huang, A. Huang, S. Jiang, H. Kawai, D. Kinzer, M. Kuball, A. Kumar, K. B. Lee, X. Li, D. Marcon, M. März, R. McCarthy, G. Meneghesso, M. Meneghini, E. Morvan, A. Nakajima, E. M. S. Narayanan, S. Oliver, T. Palacios, D. Piedra, M. Plissonnier, R. Reddy, M. Sun, I. Thayne, A. Torres, N. Trivellin, V. Unni, M. J. Uren, M. Van Hove, D. J. Wallis, J. Wang, J. Xie, S. Yagi, S. Yang, C. Youtsey, R. Yu, E. Zanoni, S. Zeltner, and Y. Zhang, "The 2018 GaN power electronics roadmap," J. Phys. D Appl. Phys. **51**, 163001 (2018).
[3]H. Fu, X. Huang, H. Chen, Z. Lu, I. Baranowski, and Y. Zhao, "Ultra-low turn-on voltage and on-resistance vertical GaN-on-GaN Schottky power diodes with high mobility double drift layers," Appl. Phys. Lett. **111**, 152102 (2017).
[4]D. Ji, M. A. Laurent, A. Agarwal, W. Li, S. Mandal, S. Keller, and S. Chowdhury, "Normally OFF trench CAVET with active Mg-doped GaN as current blocking layer," IEEE Trans. Electron Devices **64**, 805 (2017).
[5]H. Liu, H. Fu, K. Fu, S. R. Alugubelli, P.-Y. Su, Y. Zhao, and F. A. Ponce, "Non-uniform Mg distribution in GaN epilayers grown on mesa structures for applications in GaN power electronics," Appl. Phys. Lett. **114**, 082102 (2019).
[6]U. Kaufmann, P. Schlotter, H. Obloh, K. Köhler, and M. Maier, "Hole conductivity and compensation in epitaxial GaN:Mg layers," Phys. Rev. B **62**, 10867 (2000).
[7]K. Fu, H. Fu, H. Liu, S. R. Alugubelli, T.-H. Yang, X. Huang, H. Chen, I. Baranowski, J. Montes, F. A. Ponce, and Y. Zhao, "Investigation of GaN-on-GaN vertical *p-n* diode with regrown *p* -GaN by metalorganic chemical vapor deposition," Appl. Phys. Lett. **113**, 233502 (2018).
[8]S. J. Pearton, C. B. Vartuli, J. C. Zolper, C. Yuan, and R. A. Stall, "Ion implantation doping and isolation of GaN," Appl. Phys. Lett. **67**, 1435 (1995).
[9]J. Cazaux, "From the physics of secondary electron emission to image contrasts in scanning electron microscopy," J. Electron Microsc. **61**, 261 (2012).
[10]J. R. Dennison, A. Sim, and C. D. Thomson, "Evolution of the electron yield curves of insulators as a function of impinging electron fluence and energy," IEEE Trans. Plasma Sci. **34**, 2204 (2006).
[11]H. Seiler, "Secondary electron emission in the scanning electron microscope," J. Appl. Phys. **54**, R1 (1983).
[12]D. D. Perovic, M. R. Castell, A. Howie, C. Lavoie, T. Tiedje, and J. S. W. Cole, "Field-emission SEM imaging of compositional and doping layer semiconductor superlattices," Ultramicroscopy **58**, 104 (1995).
[13]C. P. Sealy, M. R. Castell, and P. R. Wilshaw, "Mechanism for secondary electron dopant contrast in the SEM," J. Electron Microsc. **49**, 311 (2000).
[14]J. Goldstein, *Scanning Electron Microscopy and X-ray Microanalysis*, 4th ed. (Springer Science, New York, 2017), p. 88.
[15]D. C. Joy, "Control of charging in low-voltage SEM," Scanning **11**, 1 (1989).
[16]A. K. W. Chee, "Enhancing doping contrast and optimising quantification in the scanning electron microscope by surface treatment and Fermi level pinning," Sci. Rep. **8**, 5247 (2018).
[17]M. El-Gomati, F. Zaggout, H. Jayacody, S. Tear, and K. Wilson, "Why is it possible to detect doped regions of semiconductors in low voltage SEM: A review and update," Surf. Interface Anal. **37**, 901 (2005).
[18]D. Venables, "Secondary electron imaging as a two-dimensional dopant profiling technique: Review and update," J. Vac. Sci. Technol. B **16**, 362 (1998).
[19]A. K. W. Chee, "Quantitative dopant profiling by energy filtering in the scanning electron microscope," IEEE Trans. Device Mater. Rel. **16**, 138 (2016).
[20]I. Volotsenko, M. Molotskii, Z. Barkay, J. Marczewski, P. Grabiec, B. Jaroszewicz, G. Meshulam, E. Grunbaum, and Y. Rosenwaks, "Secondary electron doping contrast: Theory based on scanning electron microscope and kelvin probe force microscopy measurements," J. Appl. Phys. **107**, 014510 (2010).
[21]Y. Zhao, H. Fu, G. T. Wang, and S. Nakamura, "Toward ultimate efficiency: Progress and prospects on planar and 3D nanostructured nonpolar and semipolar InGaN light-emitting diodes," Adv. Opt. Photonics **10**, 246 (2018).
[22]L. Reimer and C. Tollkamp, "Measuring the backscattering coefficient and secondary electron yield inside a scanning electron microscope," Scanning **3**, 35 (1980).
[23]J. E. Yater, J. L. Shaw, K. L. Jensen, D. W. Feldman, N. Moody, and P. G. O'Shea, in *2006 IEEE International Vacuum Electronics Conference Held Jointly with 2006 IEEE International Vacuum Electron Sources* (IEEE, Monterey, CA, USA, 2006), pp. 433–434.

[24]G. F. Dionne, "Origin of secondary-electron-emission yield-curve parameters," J. Appl. Phys. **46**, 3347 (1975).
[25]A. Shih, J. Yater, P. Pehrsson, J. Butler, C. Hor, and R. Abrams, "Secondary electron emission from diamond surfaces," J. Appl. Phys. **82**, 1860 (1997).
[26]J. P. Long and V. M. Bermudez, "Band bending and photoemission-induced surface photovoltages on clean n- and p-GaN (0001) surfaces," Phys. Rev. B **66**, 121308 (2002).
[27]K. M. Tracy, W. J. Mecouch, R. F. Davis, and R. J. Nemanich, "Preparation and characterization of atomically clean, stoichiometric surfaces of *n*- and *p*-type GaN(0001)," J. Appl. Phys. **94**, 3163 (2003).
[28]C. I. Wu, A. Kahn, N. Taskar, D. Dorman, and D. Gallagher, "Gan (0001)-(1×1) surfaces: Composition and electronic properties," J. Appl. Phys. **83**, 4249 (1998).
[29]C. G. Van de Walle and D. Segev, "Microscopic origins of surface states on nitride surfaces," J. Appl. Phys. **101**, 081704 (2007).
[30]S. L. Elliott, R. F. Broom, and C. J. Humphreys, "Dopant profiling with the scanning electron microscope—A study of Si," J. Appl. Phys. **91**, 9116 (2002).
[31]P. Kazemian, "Effect of experimental parameters on doping contrast of Si p-n junctions in a FEG-SEM," Microelectron. Eng. **73–74**, 948 (2004).
[32]L. Chernyak, A. Osinsky, V. Fuflyigin, and E. F. Schubert, "Electron beam-induced increase of electron diffusion length in -type GaN and AlGaN/GaN superlattices," Appl. Phys. Lett. **77**, 875 (2000).
[33]H. Fu, K. Fu, X. Huang, H. Chen, I. Baranowski, T.-H. Yang, J. Montes, and Y. Zhao, "High performance vertical GaN-on-GaN p-n power diodes with hydrogen-plasma-based edge termination," IEEE Electron Device Lett. **39**, 1018 (2018).